Structure of the $P_{11}(1440\ \mathrm{MeV})$ resonance from α-p and π-N scattering

H. P. Morsch
Institut für Kernphysik, Forschungszentrum Jülich, D-52425 Jülich, Germany

P. Zupranski
Soltan Institute for Nuclear Studies, P1-00681 Warsaw, Poland

(Received 19 July 1999; published 29 December 1999)

To understand the various results on the $N^*(1440\ \mathrm{MeV})$ resonance in a consistent way, the data on α-p scattering at $E_\alpha = 4.2$ GeV were reanalyzed assuming projectile and target excitation, and their interference. A quantitative fit of the spectrum is obtained, assuming for the N^* mass distribution a threshold modified Breit-Wigner shape with momentum-dependent width and resonance parameters $M = 1390 \pm 20$ MeV and $\Gamma = 190 \pm 30$ MeV. This, however, is not consistent with the data on π-N scattering which, in general, require a higher resonance mass and a larger width. Both systems, α-p and π-N, can be described consistently in a T-matrix formalism, assuming *two structures* in the $P_{11}(1440\ \mathrm{MeV})$ resonance, from which only the first one is observed in α-p. For this structure the elastic π-N width is small and the decay into the $2\pi(s)$-N channel is large. This strongly supports the conclusions drawn from α-p scattering. The second structure at higher mass has a strong decay into the $\pi\Delta$ channel and can be well understood as a second-order excitation of the $\Delta(1230\ \mathrm{MeV})$. The two resonance picture of the $P_{11}(1440\ \mathrm{MeV})$ resonance is supported by γ-induced reactions; no evidence is found for the first N^*, however, the second resonance is observed (although more or less obscured by nonresonant π-Δ production). A further crucial test of the existence of two structures in the Roper resonance is provided by exclusive α-p experiments; a N^* decay pattern should be found quite different from π-N with a very strong 2π decay.

PACS number(s): 25.55.Ci, 25.10.+s, 14.20.Gk

I. INTRODUCTION

The first N^* resonance at about 1440 MeV is in many respects a very interesting and important resonance. At this energy a P_{11} resonance has been deduced from phase-shift analyses [1–6] of elastic π-N scattering (Roper resonance). Although this resonance has never been seen directly in experimental spectra, it is a rather well established four star resonance. Its mass distribution is quite different from a normal Breit-Wigner form and has an unusually large width (as compared to neighboring resonances). Resonance parameters extracted from the different observables (see Refs. [1–6]) are not consistent. From a fit of the resonance in the total π-N cross section, resonance parameters M and Γ are obtained which are about 1470 and 350 MeV, respectively. A lower mass and a smaller width, about 1375 and 180 MeV, respectively, is suggested from the speed [1,7] (derivative of the scattering amplitude T with respect to the mass $|dT/dm|$) which shows a beautiful peak structure centered at about 1370 MeV. This resonance has also an anomalous behavior [7] in $\mathrm{Im}\,T^{\mathrm{in}}$, which describes the absorption from the elastic channel: instead of a peak as observed for other resonances, only a falloff to lower absorption is found. The P_{11} resonance is dominant in the elastic π-N channel; the inelasticities into $2\pi(s)$-N (2π coupled to isospin$=0$) and π-Δ, studied in the π-$N \rightarrow \pi\pi N$ reaction [8,9], are on the order of 10–20 %. In addition a small decay into ρ-N has been deduced [3,8].

More recently, a resonance in the same mass region has been observed [10] in α-p scattering (Saturne resonance). With the quantum numbers $(J,I)^P = (1/2,1/2)^+$ this resonance is seen in α-p scattering as a monopole excitation ($L=0$) without change of spin and isospin ($\Delta S = 0$, $\Delta I = 0$). In comparison with an energy-weighted operator sum rule this excitation has been found to be quite strong [11]; therefore, it has been interpreted as a compression or breathing mode, from which the nucleon compressibility has been deduced.

Theoretically, a $N^*(1/2,1/2)^+$ resonance at low excitation energy is of particular interest. In the constituent quark model [12] such a resonance corresponds to a $1s \rightarrow 2s$ quark excitation which should lie at an excitation energy of about 1 GeV. Therefore, attempts in this model to bring down the excitation energy significantly were not very successful. The inclusion of a three-body force [13] gives a much better description. Recently, in the context of chiral symmetry conservation a meson-exchange interaction has been employed, assuming that the massive quarks interact by the exchange of mesons [14]. In this model the $N^*(1/2,1/2)^+$ comes down to the experimental value. Interestingly, also in other chiral models as, e.g., in the Skyrmion model [15] (which treats the baryon structure as a mesonic field), a monopole mode is the lowest excitation of the baryon. Finally, it has been speculated that this resonance might correspond to a hybrid structure [16].

In the present paper an attempt is made to understand the results for π-N and α-p scattering in a consistent way and to resolve the above-mentioned problems in π-N. In Sec. II the description of the α-p spectrum is presented. Then, realistic resonance forms are given in Sec. III in a T-matrix approach. Assuming one resonance only, this yields results which are not consistent for the two scattering systems. In Secs. III and IV a quantitative description is discussed in a two-resonance model. Calculations of resonant and nonresonant $\pi\Delta$ produc-

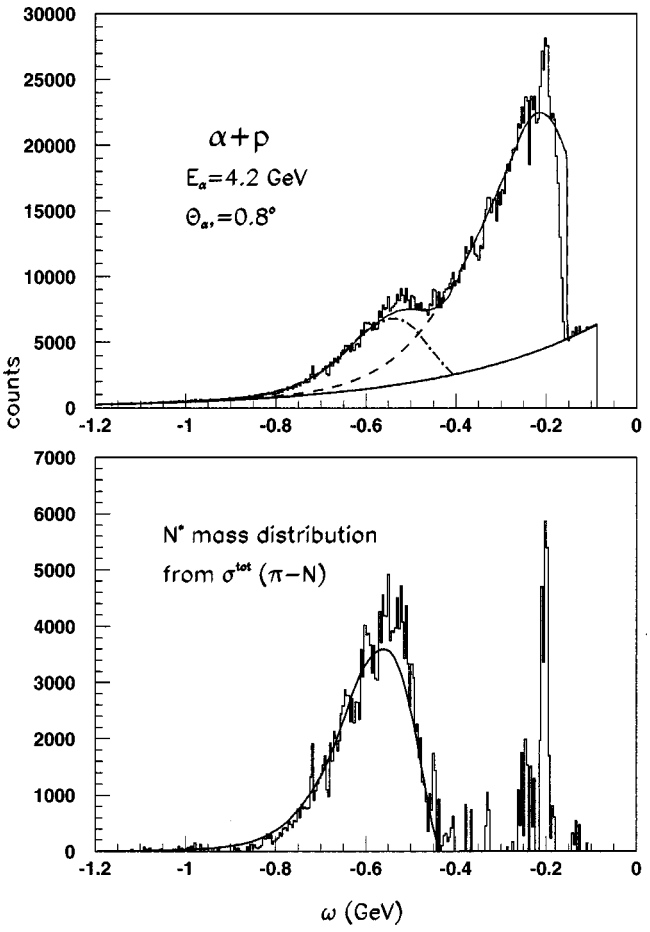

FIG. 1. Calculated missing energy spectra of inelastic α-p scattering using a mass distribution from the π-N total P_{11} cross sections (Roper resonance) in comparison with the data (slightly corrected spectrum from Ref. [10] with an exponential collimator background indicated by the solid line, see Ref. [17]). Upper part: total spectrum in comparison with the contribution from projectile excitation (1), dashed line, N^* excitation (2), dot-dashed line, and the sum of target and projectile excitation, solid line. Lower part: background and projectile excitation subtracted from the experimental data in comparison with the sum of N^* target excitation and interference term (solid line).

tion in a folding approach are presented in Sec. V and finally a comparison is made with γ-N in Sec. VI.

II. DESCRIPTION OF THE α-p SPECTRUM

We performed calculations of energy-loss spectra for $\alpha\text{-}p \rightarrow \alpha' + X$, using different N^* mass distributions. In order to obtain quantitative comparison with the experimental data in Ref. [10], a smooth instrumental background has to be subtracted, which originates from the entrance collimator of the SPES4 spectrometer. The existence of such a background, which is well approximated [17] by an exponential form, has been established in more recent experiments and is apparent in two-dimensional energy versus momentum spectra of the scattered α particle. Figure 1 shows an experimental spectrum (which is quite similar to that shown in Ref. [10]) together with an exponential background fit.

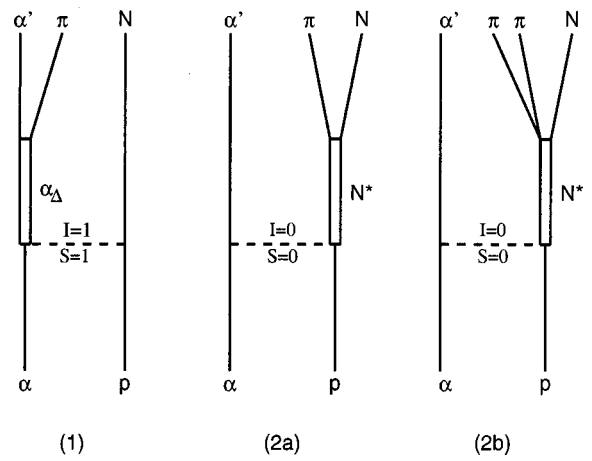

FIG. 2. Reaction graphs contributing to α-p scattering: (1) excitation of the projectile, (2) target excitation.

Similar to previous calculations [10,18,19], for the description of the spectrum we assumed two contributions, (1) Δ excitation in the projectile (which decays by coherent pion emission [18]), and (2) excitation of the N^* resonance in the proton, which can decay by one and two pions. These reaction graphs are indicated in Fig. 2. The importance of the interference between graphs (1) and (2a) has been pointed out in Ref. [19] and has been included in our calculations. Other reaction graphs have been estimated to be almost two orders of magnitude smaller [19] and have therefore been omitted.

Using the Monte Carlo method, double differential cross sections $d^2\sigma_{1,2}/(d\Omega d\omega)$ were calculated for processes (1) and (2); ω is the energy transfer between the incoming and outgoing α particle, $\omega=(E_{\alpha'}\text{-}E_{\alpha})$. If we approximate the inclusive amplitudes for $\alpha\text{-}p \rightarrow \alpha' + X$ by

$$A_{1,2} = a_{1,2} \exp(-i\phi_{1,2}) fps_{1,2}(\omega),$$

this yields

$$d^2\sigma_{1,2}/(d\Omega d\omega) = a_{1,2}^2 \cdot fps_{1,2}^2(\omega),$$

with the interference term

$$d^2\sigma_{\rm int}/(d\Omega d\omega) = 2a_1 a_2 \alpha \cos(\phi_1 - \phi_2) \cdot fps_1(\omega) fps_2(\omega).$$

The factor $\alpha(\leqslant 1)$ accounts for the amount of coherence between the inclusive amplitudes from (1) and (2). Because the contribution (1) is due to coherent π production from Δ excitation of the projectile, only the part of N^* excitation which decays into π-N (2a) gives rise to interference, therefore $\cos(\phi_1-\phi_2)=B_{\pi N}$, where $B_{\pi N}$ is the N^* decay branching ratio into π-N. The amplitudes a_1 and a_2 as well as $\alpha\cos(\phi_1-\phi_2)$ were adjusted to the experimental spectrum.

The phase-space functions $fps_{1,2}(\omega)$ were calculated within the appropriate kinematics using the routine GENBOD, assuming resonance mass distributions (discussed below) and a cutoff in the four-momentum transfer t [in units of $(\mathrm{GeV}/c)^2$] given by the inelastic form factor $F(t)$. The inelastic form factor is approximated by two exponentials $F(|t|)^2=\exp(-k_1|t|)+\exp[-k_2|t|-(k_1-k_2)t_0]$ with values of

k_1 and k_2 of 29 and 10 $(\mathrm{GeV}/c)^{-2}$, respectively, and $t_0 = 0.25\,(\mathrm{GeV}/c)^2$, to be consistent with the overall features of elastic scattering. $F(t)$ represents the overlap of the relative wave function between the α particle and nucleon in the initial and final state. For small momentum transfers this was calculated in the distorted-wave Born approximation approach (see Ref. [11]) and agrees well with the slope parameter k_1. Consistent with the conclusions of Ref. [19] the falloff of the angular distribution is essentially determined at these incident energies by the form factor and the available phase space.

It should be noted that the present approach should give spectral shapes very similar to those obtained within the meson-exchange approach (Refs. [18,19]). The additional q dependence in the vertex form factors of this model is included in our calculations implicitly in the adjusted form factor slope k. For projectile excitation (1) the spectral shape is essentially determined by the Lorentz boost in the moving system which shifts the resonance close to threshold; therefore, for Δ excitation of the projectile the spectral shapes obtained in Refs. [10], [18], and [19] have to be very close. The falloff towards larger energy transfers is entirely determined by the form factor. Different from this, the spectral shape for target excitation (2) is sensitive to the N^* mass distribution.

In a first calculation, for the N^* mass distribution $\sigma(m)$ the average total P_{11} cross section was used from the π-N phase-shift analyses [1–6] (see Sec. III). A missing energy spectrum of α-p scattering is obtained which is compared to the experimental data in Fig. 1 (in the lower part the background as well as the contribution due to projectile excitation is subtracted). The description of the data is quite similar to that obtained in Ref. [19], also with negative sign and about the same height of the interference term. Using $B_{\pi N} = 0.6$–0.7 from Refs. [1–6] this gives a rather small value of $\alpha \sim 0.3$ (see the discussion in Sec. IV A). Further, it should be noted that in both calculations the resonance peak is wider than observed experimentally.

III. RESONANCE FORMS FOR π-N AND α-p IN A T-MATRIX APPROACH

For a partial wave with angular momentum l the π-N scattering cross section is given by

$$\sigma_l = (2l+1)4\pi/k^2 \cdot |T_l|^2,$$

where the mass dependence of the π-N amplitude T_l may be given by resonances and a background $T_l(m) = \Sigma_i T_l^i(m) + B(m)$. In a realistic description $T_l^i(m)$ may be given by momentum-dependent Breit-Wigner forms with threshold cutoff functions:

$$T_l^i(m) = \mathrm{thres}_i^{n\pi}(m)\,\frac{(\Gamma_i^{\mathrm{el}}/\Gamma_i)\cdot\Gamma_i(m)/2}{M_i - m - i\Gamma_i(m)/2} \qquad (1)$$

with

$$\Gamma_i(m) = \left(\frac{q_\pi(m)}{q_\pi(M_i)}\right)^{(2l+1)m_i^{\mathrm{cut}}}\Gamma_i, \qquad (2)$$

where $q_\pi(m)$ is the pion c.m. momentum. The $q^{(2l+1)}$ dependence of the width is due to the centrifugal barrier. With increasing mass the barrier influence decreases and we need a cutoff m^{cut}; this is important to obtain the observed resonance falloff to larger masses. For the N^* resonances a very smooth cutoff is needed which may be given by $m_i^{\mathrm{cut}} = [1-(\beta-1)/(\beta+1)]$ with $\beta = e^{m_i^{\mathrm{scal}} C_{\mathrm{cut}}}$ and $m_i^{\mathrm{scal}} = (m - m_{\mathrm{thr}})/(M_i - m_{\mathrm{thr}})$. With such a mass cutoff, however, the shape of the $\Delta(1230)$ resonance is not well described. Here, $m_i^{\mathrm{cut}} = e^{-m_i^{\mathrm{scal}} C_{\mathrm{cut}}}$ gives an excellent description of both the resonance shape [4,6] and the speed [7]. The different mass cutoffs needed for Δ and N^* reflect the differences in the decay properties of these resonances.

Threshold functions $\mathrm{thres}_i^{n\pi}(m)$ for 1 and 2 pion production (which go from zero at threshold to one at higher mass) are essential for a correct description of the amplitudes. They are approximated by $\mathrm{thres}_i^{n\pi}(m) = [(\beta-1)/(\beta+1)]$ with $\beta = e^{m_i^{\mathrm{scal}} C_{\mathrm{thr}}}$. For the description of elastic π-N scattering (which gives also the total inelastic cross section) only 1π threshold functions are needed, whereas 2π threshold functions are required for the description of the production cross sections of inelastic channels. A quantitative description of the 2π-threshold cross sections in Ref. [20] is obtained using values of C_{thr} of 6–8. Finally, background amplitudes for n (1 and 2) π production in the form $B_{n\pi}(m) = b\,\mathrm{thres}^{n\pi}(m)\cdot q_{n\pi}/m$ (from Ref. [21]) are added.

Here it should be noted that for the inclusion of threshold, angular momentum, and background effects different modifications of the Breit-Wigner form have been used by different authors (see, e.g., Refs. [4,6]). In our approach we have aimed at a realistic physical picture, which allows us to describe different reactions and exit channels consistently.

The speed is given by $|dT_l(m)/dm|$, this quantity is very sensitive to changes of the scattering amplitudes. Because of this, speed provides a sensitive test of the resonance form, and we can expect a reasonable description of this quantity only, if all details of the resonance description are correct.

Directly related to the absorption is $\mathrm{Im}\,T_l^{\mathrm{in}}(m) = \mathrm{Im}\,T_l(m) - |T_l(m)|^2 = 1/4(1-\eta_l^2)$, where η_l is the absorption parameter (unitarity demands $\mathrm{Im}\,T_l^{\mathrm{in}} \leqslant 0.25$).

The total cross section is given by $\sigma_l^{\mathrm{tot}}(m) = (2l+1)4\pi/k^2\,\mathrm{Im}\,T_l(m)$, the inelastic cross sections by $\sigma_l^{\mathrm{inel}}(m) = (2l+1)4\pi/k^2\,\mathrm{Im}\,T_l^{\mathrm{in}}(m)$. The partial inelastic cross sections (2π production) are given by $\sigma_{l,i}^{\mathrm{inel}}(m) = (2l+1)4\pi/k^2[\mathrm{thres}_i^{2\pi}(m)/\mathrm{thres}_i^{n\pi}(m)](\Gamma_i^{\mathrm{out}}/\Gamma_i)\mathrm{Im}\,T_{l,i}^{\mathrm{in}} \times(m)$. The differential cross section for α-p scattering is related to the π-$N \to 2\pi(s)$-N production (same quantum numbers) and is given for a resonance i by

$$d\sigma/d\Omega_i(\omega) \sim (2l+1)4\pi/k^2[\mathrm{thres}_i^{2\pi}(m)/\mathrm{thres}_i^{n\pi}(m)] \times(\Gamma_i^{\mathrm{out}^2}/\Gamma_i\Gamma_i^{\mathrm{el}})\mathrm{Im}\,T_{l,i}^{\mathrm{in}}(m)F(t),$$

where $F(t)$ is the inelastic form factor discussed in Sec. II.

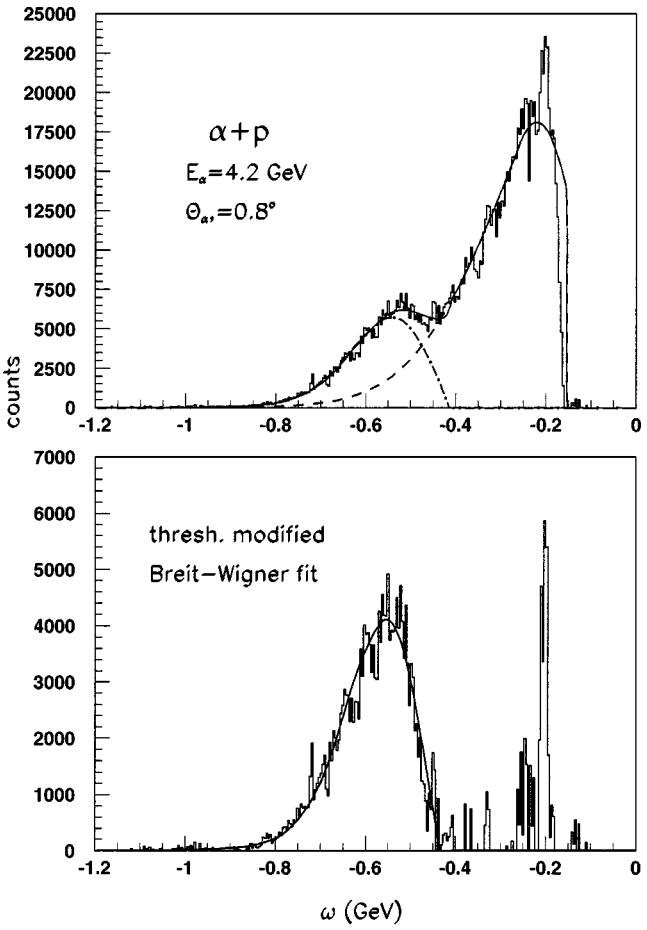

FIG. 3. Same as Fig. 1 (with collimator background subtracted) but assuming a fitted N^* mass distribution with the resonance parameters in Table I.

A good fit of the Saturne resonance (see Fig. 3) is obtained using values of M and Γ of about 1.39 and 0.19 GeV, respectively. For the interference term (which is only related to the π-N amplitude) a value of $\alpha\cos(\phi_1-\phi_2)$ between -0.16 and -0.25 (with a slight preference for the larger negative values) is obtained. It is clear that a resonance with these parameters fails to describe the overall features of the P_{11} structure seen in π-N scattering; in general higher centroid energies and larger widths are needed [2–6]. Only the peak in the inelastic $2\pi(s)$-N production data from Ref. [8] is well described (see below); this is expected due to a similar L coupling in α-p and $2\pi(s)$-N production.

Description of the Roper resonance as a double-resonance structure

The above results suggest that the structures observed in α-p and π-N are not identical. The scattering of α particles is very selective, exciting only isoscalar, non-spin-flip structures. Differently, π-N scattering is a resonant reaction which shows very little selectivity. Indeed, in this system the decay of the Roper resonance into $\pi\Delta$ is quite strong at higher mass, which could indicate a coupling to the Δ degree of freedom (second-order excitation of the Δ resonance), which should not be observed in α-p scattering.

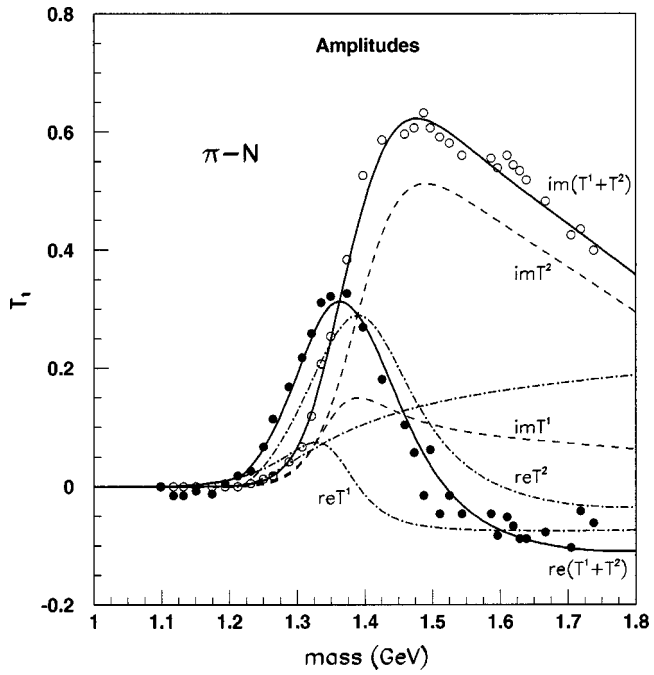

FIG. 4. π-N amplitudes T_1 (real and imaginary part given by solid and open points, respectively) from Refs. [4,6] in comparison with our fits (solid lines). The separate amplitudes for the first and second resonance are given by the broken lines (real, dot-dashed lines; imaginary, dashed lines). The background term starting at the 2π threshold is also shown by a dot-dashed line.

The different results may be reconciled in a two-resonance picture of the Roper resonance, assuming that in α-p scattering only the lower N^* resonance is excited. Using the modified Breit-Wigner forms given in Eqs. (1) and (2), the π-N amplitudes, speed, and cross sections were fitted under the constraint, that the resonance parameters of the first resonance are already fixed by the description of α-p scattering. The required mass and width of the second resonance is about 1.48 and 0.4 GeV, respectively. Interestingly, a good description of the amplitudes is only obtained, if for the second resonance a 2π threshold function in Eq. (1) is used. This suggests strongly that this resonance is intrinsically related to a 2π-N structure. A real background which starts only at the 2π threshold is added, with an amplitude necessary to describe the negative part of the real amplitude in the region above the resonance.

A comparison of our calculations with the π-N data is made in Figs. 4–8. For the π-N amplitudes (which show larger deviations) a comparison in Fig. 4 is made only with the more recent data of Refs. [4] and [6]; however, for the other quantities all results of Refs. [1–8] are used and a quantitative description of the cross sections is emphasized. The resulting parameters in the calculations are given in Table I.

We obtain a good description of the speed plot in Fig. 5. Here, it is of interest to ask why the speed shows such a sharp peak for a double-resonance structure, where one resonance lies at a rather high mass. The crucial point is the 2π threshold behavior of the second resonance which brings the speed peak below 1.4 GeV. The speed for the two resonances

TABLE I. P_{11} resonance parameters deduced using threshold modified Breit-Wigner forms in Eqs. (1) and (2). The values in (brackets) indicate the estimated uncertainties.

Parameter	Resonance (first)	Resonance (second)
Mass (GeV)	1.39 ($\pm$0.02)	1.48 ($\pm$0.03)
Width (GeV)	0.19 ($\pm$0.02)	0.38 ($\pm$0.05)
$B_{\pi N}(\Gamma^{\rm el}/\Gamma)$	0.15 ($\pm$0.10)	0.53 ($\pm$0.15)
$B_{2\pi N}(\Gamma^{\rm inel}/\Gamma)$	0.88 ($\pm$0.15)	0.66 ($\pm$0.20)
Threshold	1π	2π
$C_{\rm thres}$	8	4
$C_{\rm cut}$	0.1	0.2
backgr (2π)		0.55
Observed in the reactions	α-p π-N elast. π-$N\rightarrow 2\pi(s)$-N	π-N elast. π-$N\rightarrow\pi\Delta$

separately is given in Fig. 5 by the dashed lines.

The features of Im $T^{\rm in}$ in Fig. 6 clearly support the two-resonance picture. For one resonance only, Im $T^{\rm in}$ shows always a peak structure (as shown by the dashed line for the first resonance). Therefore, the anomalous behavior [7] of the Roper resonance, as discussed in Sec. I, supports clearly the presence of a double structure. Our results are very close to those of Refs. [4,6]. The inelastic data of Ref. [8] (solid points) show a sharp falloff from 1.6 to 1.7 GeV. As our calculations are constrained by the total cross sections which show a smooth falloff, such a behavior cannot be reproduced (see the discussion of the inelastic data below).

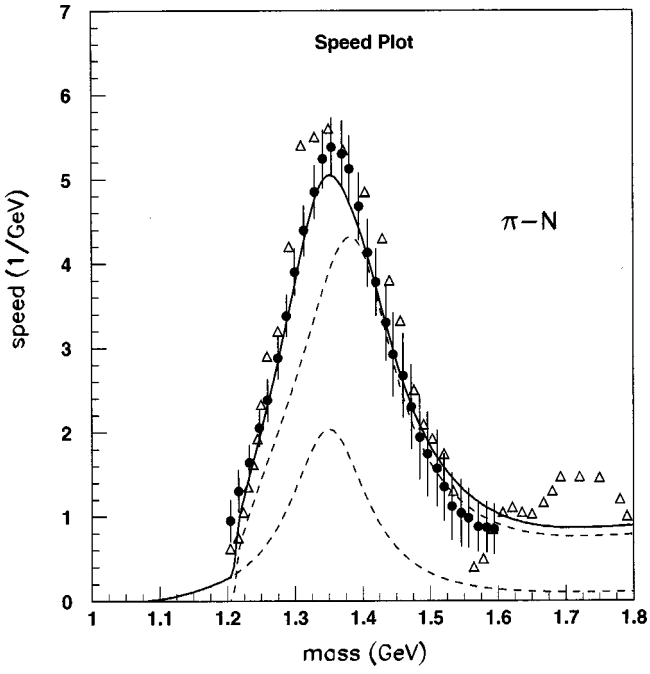

FIG. 5. Calculated speed (solid line) in comparison with the data from Ref. [1] (triangles) and Refs. [4,6] (solid points). The error bars indicate the scatter of different solutions. The speed for the separate resonances is shown by the dashed lines.

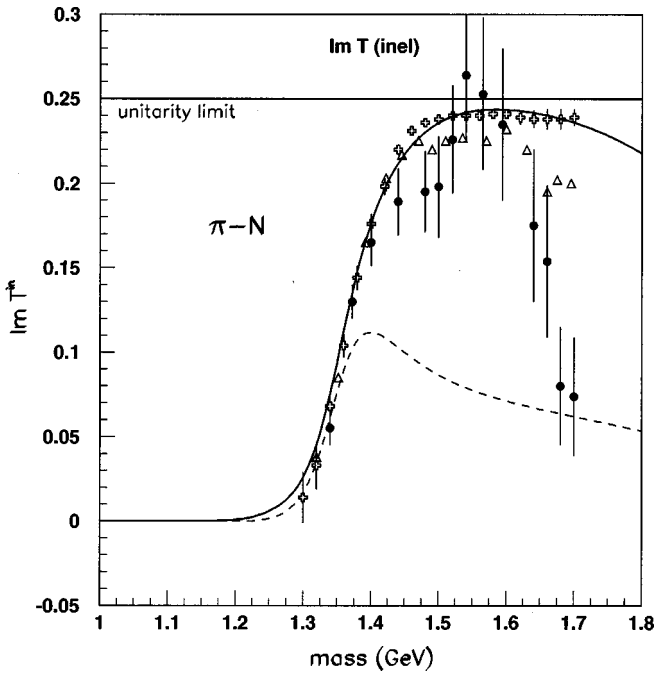

FIG. 6. Calculated Im $T^{\rm in}$ in comparison with the results from Ref. [1] (triangles), Ref. [4] (open crosses), and Ref. [8] (solid points with error bars). Im $T^{\rm in}$ for the first resonance alone is given by the dashed line.

The total and inelastic cross sections are compared to the average data [1–6] in Fig. 7. The partial inelastic cross sections for the first resonance are given by the dashed line. From this the total branching ratios in π-N scattering are 58, 16, and 26 % for π-N elastic, $2\pi(s)$-N, and $\pi\Delta$, respectively.

The partial cross sections for the first and second resonance are compared in Fig. 8 to the inelastic data of Ref. [8]. The open and square points in the upper part are obtained from a different extraction of the inelastic π-$N\rightarrow 2\pi(s)$-N cross sections. The two first points close to threshold in the upper part represent data from Ref. [20]. The partial cross sections for the first resonance give a good description of the π-$N\rightarrow 2\pi(s)$-N cross sections, whereas the data for π-$N\rightarrow\pi\Delta$ are reasonably well described by the partial cross sections of the second resonance. This indicates strongly that the two resonances decay mainly into different channels; this is schematically shown in the upper part of Fig. 9. The dashed line in the lower part of Fig. 8 is obtained by subtracting the first resonance from the total inelastic cross sections. The fact that both lines are close to each other shows the consistency of our description.

The strong falloff of the inelastic data [8] for π-$N\rightarrow\pi\Delta$ to large masses (solid points in the lower part of Fig. 8) is not consistent with the total inelastic cross sections. This could indicate that at higher mass the cross section is taken over by another structure, the P_{11}(1710 MeV) resonance, which may decay much weaker into the $\pi\Delta$ channel. Indications of the P_{11}(1710 MeV) resonance in π-N has been found [3] (with sizeable ρN decay) and is also visible in the speed plot of Ref. [1]. In the present work this effect is not taken into consideration, which could result in too large a

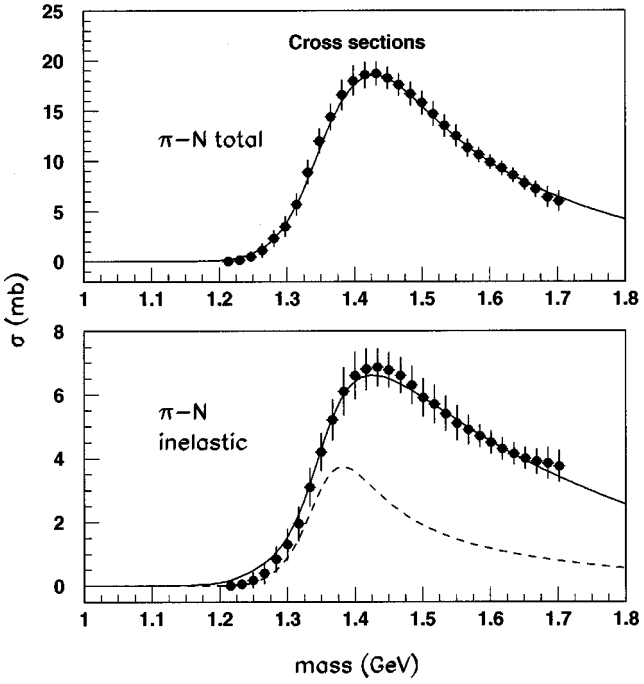

FIG. 7. P_{11} total and inelastic cross sections (average from Refs. [1–6] with the uncertainties from the different solutions) together with our fit (solid lines). The dashed line in the lower part indicate the partial cross section for the first resonance.

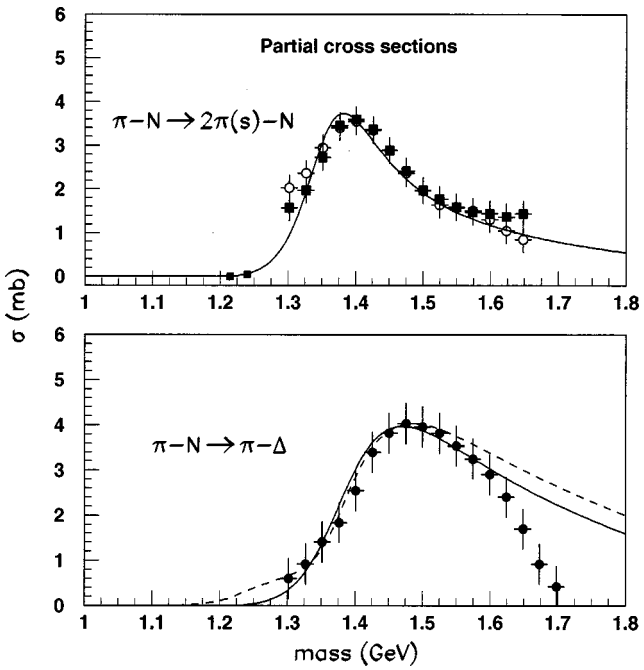

FIG. 8. Partial inelastic π-N cross sections for the first and second resonance (solid lines) in comparison with the data [8] on π-$N \rightarrow 2\pi(s)$-N (upper part) and π-$N \rightarrow \pi\Delta$ (lower part). Error bars of 10% of the cross section at maximum are assumed. The two data points in the upper part close to threshold are from Ref. [20]. The dashed line shows the difference in cross section between the total inelastic yield and that of the first resonance.

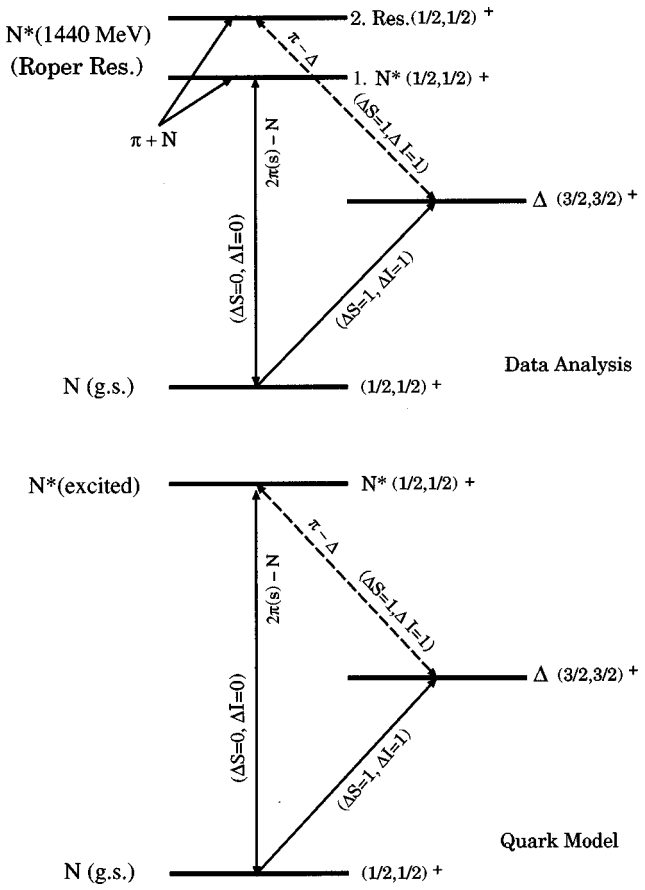

FIG. 9. Level and dominant transition scheme of the different structures involved. Upper part, our results; lower part, quark model prediction.

width extracted for the second resonance structure.

IV. RESULTS

In the above analysis of the Roper resonance in terms of two resonance structures with different decays (as shown in the upper part of Fig. 9), *all inconsistencies* between the different data sets are resolved. Only one resonance (that at lower mass) should be identified with a low-lying $(J,I)^P = (1/2,1/2)^+$ state predicted in baryon models [12–15]. The other resonance may be understood as a more complicated P_{11} structure, most likely related to the Δ degree of freedom. In the following the results for each resonance are compared with possible interpretations for its structure.

A. Structure of the first (Saturne) resonance

From our fits of the π-N data we obtain a small elastic width and a large decay branching into the $2\pi(s)$-N channel. This supports strongly the conclusions drawn from α-p scattering [10,11], that this resonance can be understood to a large extent by a monopole excitation without change of spin and isospin ($\Delta S=0$, $\Delta I=0$). This resonance may be identified with a low-lying $N^*(1/2,1/2)^+$ as predicted in baryon models [13–15].

The result of a small π-N width is also supported by the analysis of the α-p spectrum (Sec. III), in which a small

interference term with $\alpha\cos(\phi_1-\phi_2)$ of $-(0.16–0.25)$ has been deduced ($|\cos(\phi_1-\phi_2)|=B_{\pi N}$). Using a coherence factor α rather close to one (which is expected from the decay kinematics), this yields $B_{\pi N}\geqslant(0.16–0.25)$ in good agreement with the value of $B_{\pi N}$ extracted from π-N scattering (Table I). The large inelastic width makes it clear, why this resonance is so strongly excited in α-p scattering.

B. What is the structure of the second resonance?

The extracted width of about 380 MeV for this resonance is very large, significantly larger than that of any other N^* resonance up to 1800 MeV. For this exceptionally large width so far no reasonable explanation has been found. This may indicate a more complicated structure compared to other N^*'s. The nonobservation in α-p scattering and the dominant $\pi\Delta$ decay properties suggest a structure related to the Δ degree of freedom [transition with change of spin and isospin ($\Delta S=1$, $\Delta I=1$), see Fig. 9]. We can think of a second-order excitation of the $\Delta(1230\,\mathrm{MeV})$, in which this resonance is again excited by a spin-isospin operator to a $(J,I)^P=(1/2,1/2)^+$ resonance. For the $\Delta(1230\,\mathrm{MeV})$ resonance the observation of such a second-order effect is conceivable because of its strong π-N amplitudes, but we expect also a very short lifetime of this resonance, resulting in a large width.

For a discussion of such an excitation in the quark model (assuming three valence quarks), the corresponding level scheme is given in the lower part of Fig. 9. The $(1/2,1/2)^+$ state is directly excited by a $1p\rightarrow 2p$ quark transition. Further, a two-step or double-excitation via the Δ resonance leads to the same state; the corresponding operator is a quark spin-flip to the $2s$ shell. Because of this, the N^* can decay into $2\pi(s)N$ as well as in $\pi\Delta$. For the double excitation we expect a much larger resonance width (see the discussion below); therefore, the quark model picture can qualitatively explain why the Roper resonance has a very large width.

In comparing both schemes in Fig. 9 we see that the structure in the quark model is simpler than found experimentally. A splitting of the $(1/2,1/2)^+$ state in two resonances appears to be quite naturally, if in the model ground-state correlations or meson cloud effects are included. In a dynamical picture of the N^* in terms of a compressional mode [11] it is quite evident that this structure is very different from that generated by spin-flip excitations of quarks.

To see whether the picture of the second resonance in terms of a double or two-step excitation of the Δ is consistent with the data, in the next section calculations are presented in which the T-matrix amplitudes used in Sec. III are replaced by folding amplitudes which describe the double excitation explicitly. In addition possible nonresonant $\pi\Delta$ production is discussed.

V. FOLDING AMPLITUDES FOR A SECOND-ORDER Δ EXCITATION AND NONRESONANT $\pi\Delta$ PRODUCTION

T-matrix amplitudes for a double excitation of the Δ resonance may be calculated by folding the resonance amplitudes for an excited resonance (x) built on the $\Delta(1230\,\mathrm{MeV})$ with the strength distribution of the latter:

$$T_{\mathrm{so}}(m)=(-i)N\int_0^m T_x(m')\,im\,T_\Delta(m-m')\,dm'. \qquad (3)$$

The normalization factor N is obtained by requiring that the elastic and inelastic branching ratios sum up to one. The folding of the imaginary amplitudes is straightforward; however, for the real amplitudes care has to be taken to avoid cancellations between positive and negative parts. In the folding expression (3) the fact, that the lifetime of the double excitation is strongly reduced compared to single excitation, is included; this results in a very large resonance width. We have to make sure that the properties of the $\Delta(1230\,\mathrm{MeV})$ are described correctly. Using the parameters in Table II we

TABLE II. P_{11} resonance parameters assuming N^*, $\Delta(1230$ MeV), and an excited resonance x. The resulting parameters for the folded second resonance are $M=1470\pm30$ MeV and $\Gamma=360\pm50$ MeV. The values in (brackets) indicate the estimated uncertainties.

Parameter	N^* resonance	$\Delta(1230)$	x (excited)
Mass (GeV)	1.39 ($\pm$0.02)	1.232	1.19 ($\pm$0.03)
Width (GeV)	0.19 ($\pm$0.02)	0.115	0.19 ($\pm$0.05)
$B_{\pi N}$ ($\Gamma^{\mathrm{el}}/\Gamma$)	0.20 ($\pm$0.10)	$\sim$1.0	0.42 ($\pm$0.15)
$B_{2\pi N}$ ($\Gamma^{\mathrm{inel}}/\Gamma$)	0.77 ($\pm$0.20)	0.58%[a]	0.58 ($\pm$0.20)
Threshold	1π	1π	1π
C_{thres}	8	12	12
C_{cut}	0.1	0.55	0.65
Background			0.30
Backgr (2π)			0.75

[a]Decay branching in γ–N.

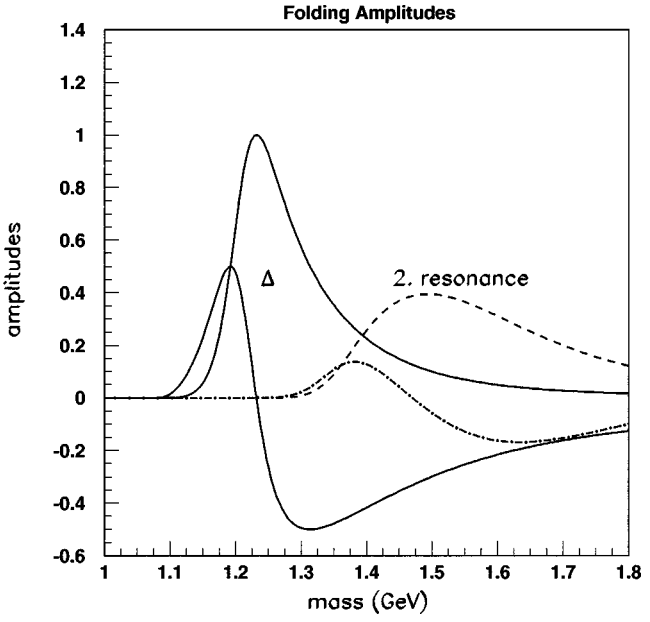

FIG. 10. Mass dependence of the Δ and folding amplitudes. Solid lines for $\Delta(1230\,\mathrm{MeV})$, dot-dashed (real part), and dashed (imaginary part) lines for the second resonance.

obtain a good description of the corresponding π-N amplitudes [1–6] (see Fig. 10) as well as the speed [7].

For the excited state x the resonance parameters are expected to be different and have to be adjusted to the data. We varied these parameters to describe the π-N data in Figs. 4–7. A good description of the peak region in the total cross sections in Fig. 7 is obtained using for x the following resonance parameters: $M=1.19-1.20\,\mathrm{GeV}$, $\Gamma=0.19-0.20\,\mathrm{GeV}$, and $\Gamma^{\mathrm{el}}/\Gamma\sim 0.50$. It appears reasonable that the deduced width is comparable to that of the first N^* resonance and that the elastic width is reduced by about a factor of 2. The resulting T-matrix amplitudes for the second resonance are also given in Fig. 10 using the resonance parameters in Table II.

Interestingly, the mass of x is quite close to that of the $\Delta(1230\,\mathrm{MeV})$, even slightly lower by about 30–40 MeV. Because of this, we may understood the second resonance as a Δ excitation of the $\Delta(1230\,\mathrm{MeV})$. This is very different from the quark model prediction: because a quark is excited to the $2s$ shell the mass of the excited state is quite high.

In the region of the second resonance a small contribution of nonresonant $\pi\Delta$ production could be expected. Such a term has been found to be very important in photoproduction (Born or contact term [22]) which, however, couples dominantly to $J=3/2^-$ (no angular momentum between π and Δ). The mass dependence of such a contribution may be obtained in a folding approach similar to Eq. (3) by folding the Δ amplitudes with a flat π distribution approximated by the used background form $B_\pi(m)$ (see Sec. III):

$$T_{\pi\Delta}(m)=p_{\pi\Delta}\int_0^m B_\pi(m')e^{-\kappa q^2}imT_\Delta(m-m')dm'. \quad (4)$$

The factor $p_{\pi\Delta}$ is the probability to produce a pion and a Δ in one interaction, $e^{-\kappa q^2}$ is a momentum cutoff which can be adjusted to the observed mass dependence. Mainly from the data of γ-induced reactions (discussed in the next section) κ is fixed to a value of 7 $(\mathrm{GeV}/c)^{-2}$.

Including such a nonresonant $\pi\Delta$ term in our calculations, we find that its contribution to the π-N P_{11} amplitudes is rather small: this component does not produce a peak in the speed plot (see Fig. 11); further, such a term contributes to P_{11} only for a relative angular momentum $L=1$ between π and Δ, which is not very likely. Results for speed and amplitudes with $p_{\pi\Delta}=3\%$ are given in Fig. 11. The speed is generally well described but fails to reproduce the mimimum in the data at about 1.6 GeV. The various quantities in Figs. 4–8 are well described (of similar or slightly better quality as in the two-resonance description in Sec. III). This confirms our interpretation of the second resonance in terms of a second-order excitation of the Δ resonance.

VI. COMPARISON WITH γ-N

In total photoabsorption the Δ resonance is strongly excited, therefore it is interesting to investigate the importance of the second resonance in photoinduced reactions. Experimentally, in these reactions [23–25] a structure is observed in the mass region in question; therefore it is important to clarify the relation of this structure to the resonances seen in π-N.

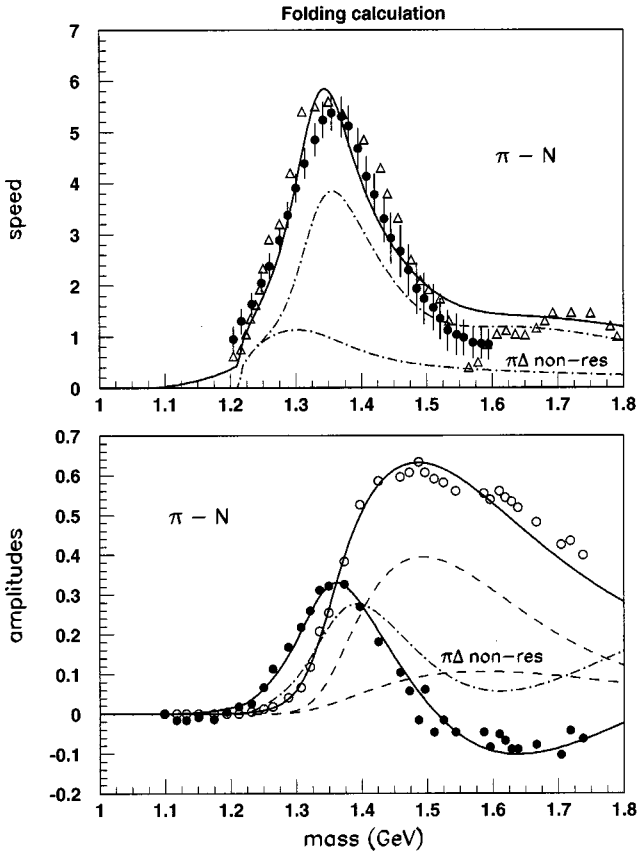

FIG. 11. Speed (upper part) and amplitudes (lower part) obtained from a fit using folding amplitudes for the second resonance and nonresonant $\pi\Delta$ contribution (broken lines). The solid lines include all components. The data points are the same as in Figs. 4 and 5.

Using the T-matrix amplitudes discussed in Sec. III, the total cross sections for photoproction are given by $\sigma^{\mathrm{tot}}_{l,\gamma}(m)=(2l+1)4\pi/k^2_\gamma(\Gamma_{\gamma-N}/\Gamma_{\pi-N})\mathrm{Im}\,T_l(m)$, further the partial inelastic cross sections (2π production) by $\sigma^{\mathrm{inel}}_{l,i,\gamma}(m)=(2l+1)4\pi/k^2_\gamma(\Gamma_{\gamma-N}\Gamma^{\mathrm{out}}_i/\Gamma^2_{\pi-N})\mathrm{Im}\,T^{\mathrm{in}}_{l,i}(m)$. Using for $(\Gamma_{\gamma-N}/\Gamma_{\pi-N})$ a value of 0.58% (from the review of particle properties) our results for excitation of the Δ and the second resonance are given in Fig. 12. These are compared to the cross sections of total photoabsorption [23] and 2π photoproduction [24].

In the $\Delta(1230\,\mathrm{MeV})$ region, our P_{33} amplitudes in Fig. 10 describe the main part of the strong peak in the total cross sections (to the strong $M1$ excitation a small $E2$ amplitude consistent with Ref. [26] is added). This is shown by the solid line in Fig. 12. In the partial wave analysis [26] of single pion photoproduction other multipole components have been deduced, e.g., rather strong E_{0^+} amplitudes, which fall off fast with increasing mass. The sum of the other multipole amplitudes (except those for the $D_{13}(1520\,\mathrm{MeV})$ resonance, which are explicitly taken into account) may be approximated for our purpose by a ''background'' contribution, given by the dot-dashed line in Fig. 12. Concerning the $M^{1/2}_{1^-}$ amplitudes (which correspond to our P_{11} amplitudes in

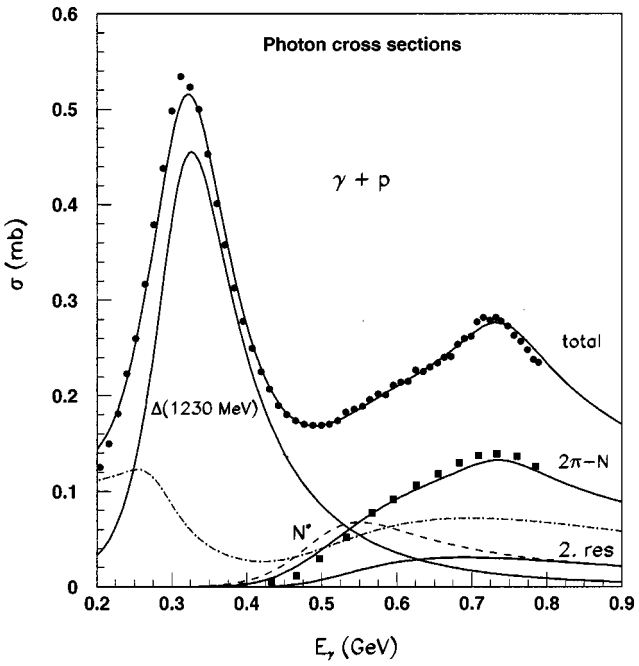

FIG. 12. Calculated cross sections of the various contributions for γ-N in comparison with total photoabsorption data (Ref. [23]) (upper points) and 2π photoproduction data (Ref. [24]) (sum over all isospin channels, given by the square points). The cross sections for the $\Delta(1230\,\mathrm{MeV})$ and the second resonance are given by the lower solid lines. The fitted multipole background is given by the dot-dashed line. The sum of the contributions from the second resonance, nonresonant $\pi\Delta$, and from the $D_{13}(1520\,\mathrm{MeV})$ resonance is compared to the 2π production data (solid line), and the sum of all contributions to the total photoproduction (upper solid line). Arbitrarily normalized cross sections for the first N^* resonance are given by the dashed line.

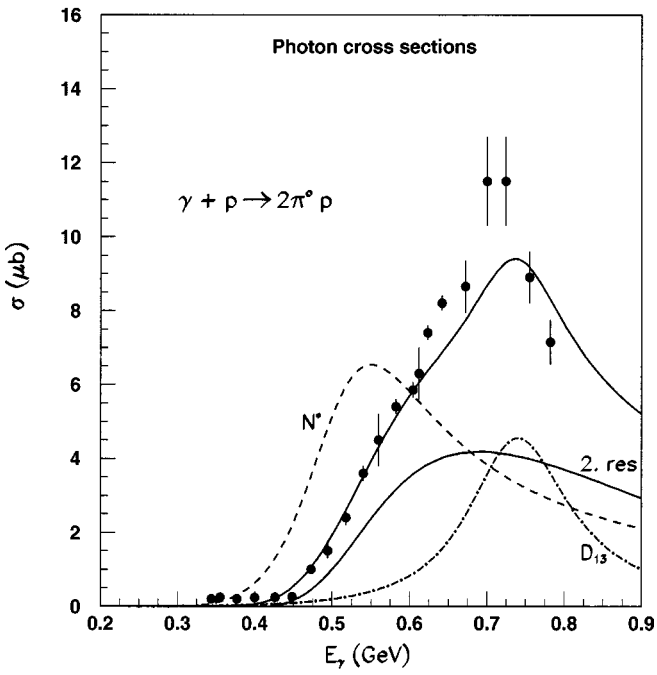

FIG. 13. Calculated cross sections for neutral 2π production with the same components as in Fig. 12 in comparison with the cross sections (Ref. [25]) for γ-$p\rightarrow 2\pi^0 p$.

π-N), it is interesting to note that in the partial wave analysis of Ref. [26] the fitted P_{11} resonance parameters, $M=1463\pm 7$ MeV, $\Gamma=360\pm 20$ MeV, and $\Gamma_\pi/\Gamma=0.68$, are in good agreement with the parameters of our second resonance (Tables I and II). However, the total cross sections calculated for this resonance, given by the lower solid line, are significantly smaller than the experimental data of 2π photoproduction [24] (square points).

Therefore, for the description of the experimental cross sections a dominant nonresonant $\pi\Delta$ contribution [22], as discussed at the end of Sec. V, is needed with a value of $p_{\pi\Delta}$ of about 20%. In this case the nonresonant amplitudes couple mainly to $J=3/2^-$ (angular momentum $L=0$ between π and Δ), which is strongly favored for this process (as compared to $J=1/2^+$ in the π-N case in Sec. V, for which the extracted probability $p_{\pi\Delta}$ was only 3%). Adding the second resonance and the coupling to the $D_{13}(1520\,\mathrm{MeV})$ resonance (discussed below), the 2π photoproduction cross sections in Fig. 12 are quite well reproduced.

The upper solid line in Fig. 12 is obtained by adding the different contributions discussed above and the $D_{13}(1520\,\mathrm{MeV})$ resonance strength. The $D_{13}(1520\,\mathrm{MeV})$ amplitudes were obtained from a fit of the π-N amplitudes [4], using the generalized Breit-Wigner form in Eqs. (1) and (2). An excellent description of the amplitudes is obtained using $M=1510\,\mathrm{MeV}$, $\Gamma=110\,\mathrm{MeV}$, $\Gamma_\pi/\Gamma=0.61$, and $C_{\mathrm{thres}}=30$; further, a mass cutoff function for the width as for the Δ resonance with $C_{\mathrm{cut}}=2.0$.

The large nonresonant $\pi\Delta$ production is expected to be strongly reduced in $2\pi^0$ production; this reaction should be therefore a much cleaner probe for the investigation of resonance effects. However, the cross sections calculated are very sensitive to the partial decay widths which are not so well known. The various components discussed above have been calculated for this channel and are compared in Fig. 13 to the experimental data [25] of the γ-$p\rightarrow\pi^0\pi^0 p$ reaction. Indeed, a large part of the cross section is described by the second resonance, assuming 85% decay into $\pi\Delta$ and 15% into $2\pi(s)N$. Adding a nonresonant $\pi\Delta$ component with a very small probability of $p_{\pi\Delta}$ of 0.5% only, a good description of the data at the lower energies is obtained. A strong peak due to the $D_{13}(1520\,\mathrm{MeV})$ resonance is obtained (see Fig. 13), assuming 45% decay both into $\pi\Delta$ and ρN and 10% into $2\pi(s)N$.

It is also important to verify, whether the first N^* (Saturne resonance) is observed in photoproduction. This resonance is strongly excited in α-p and described by an isoscalar monopole excitation; this cannot be seen in γ-N. However, in addition to the dominant $\langle r^2\rangle$ matrix element [11] a small $\langle r^2\rangle\ \sigma_1\sigma_2$ component cannot be excluded, which would be observable in γ-N. Therefore, arbitrarily normalized cross sections [using a similar photon coupling as for the second resonance] are given in Figs. 12 and 13 for this resonance by the dashed lines. The comparison with the 2π photoproduction data shows, however, that this component is strongly suppressed.

Finally, it should be mentioned that 2π production by pions and photons has been studied in a more microscopic approach (adding up to more than 40 Feynman diagrams), see Refs. [27] and [28]. More and more microscopic descriptions of the processes and structures are indispensible to reveal the origin of the resonances involved. However, in contrast to the very complex treatment using Feynman diagrams, our phenomenological *T*-matrix description has only few resonance and background components, which makes a quantitative and consistent comparison of resonance effects in different reactions much easier.

VII. SUMMARY

The detailed study of the $N^*(1/2,1/2)^+$ excitation in α-p and π-N scattering shows that by a complementary study of baryon resonances with different probes more insight into these structures can be obtained. This is very important for the Roper resonance which has a complicated structure showing up differently in various reactions. Our analysis indicates a double structure from which only the first one (Saturne resonance) is excited in α-p, the second is seen in γ-N and both are observed in π-N. The small deduced elastic width of the first resonance indicates properties quite different from other resonances, supporting the conclusion drawn from α-p scattering. This resonance may be identified with a low-lying $N^*(1/2,1/2)^+$ resonance predicted in baryon models.

Our analysis has shown that the second structure can be well described by a second-order or double excitation of the $\Delta(1230\,\mathrm{MeV})$. In this picture the large width observed experimentally is naturally explained. The splitting of the $(1/2,1/2)^+$ resonance is not understood in the simple valence quark model, for which already the low mass of this state creates a severe problem.

The present results can be tested further in exclusive α-$p \rightarrow \alpha' N^*$ experiments. As in this system the lower N^* component is excited only, branching ratios for the N^* decay are expected to be very different from those observed in π-$N \rightarrow N^*$. We should not see a strong decay into the $\pi\Delta$ channel (only possible by a small mixtures of the two resonances) and decay branchings into π-N and $2\pi(s)$-N close to the values for the first resonance given in Table I.

The structure seen in α-p scattering indicates a strong excitation of resonances in the scalar isoscalar channel which may be dominated by collective effects (compression of the mesonic cloud). Other collective modes of different multipolarity are expected in this channel which can be investigated in similar hadronic reactions at higher c.m. energies. Such a program is envisaged at COSY.

ACKNOWLEDGMENT

The authors are indebted to Professor G. Höhler for critical discussions and providing us with many details on π-N scattering.

[1] G. Höhler *et al.*, *Handbook of Pion-Nucleon scattering* (Physics Data No. 12-1) Fachinformationszentrum Karlsruhe 1979; G. Höhler (private communication).
[2] R. E. Cutkosky, C. Forsyth, R. E. Hendrick, and R. L. Kelly, Phys. Rev. D **20**, 2839 (1979).
[3] R. E. Cutkosky and S. Wang, Phys. Rev. D **42**, 235 (1990), and references therein.
[4] R. A. Arndt, I. I. Strakovsky, R. L. Workman, and M. M. Pavan, Phys. Rev. C **52**, 2120 (1995), and references therein.
[5] V. V. Abaev and S. Kruglov, Z. Phys. A **352**, 85 (1995).
[6] R. A. Arndt *et al.*, new results from SAID, 1998 (unpublished).
[7] G. Höhler and A. Schulte, πN Newslett. **7**, 94 (1992); G. Höhler, *ibid.* **9**, 1 (1993).
[8] D. M. Manley, R. A. Arndt, Y. Goradia, and V. L. Teplitz, Phys. Rev. D **30**, 904 (1984).
[9] D. M. Manley and E. M. Saleski, Phys. Rev. D **45**, 4002 (1992).
[10] H. P. Morsch *et al.*, Phys. Rev. Lett. **69**, 1336 (1992).
[11] H. P. Morsch, W. Spang, and P. Decowski, Z. Phys. A **348**, 45 (1994); H. P. Morsch, **350**, 61 (1994).
[12] See, e.g., N. Isgur and G. Karl, Phys. Rev. D **18**, 4187 (1978).
[13] B. Desplanques *et al.*, Z. Phys. A **343**, 331 (1992); F. Cano *et al.*, Nucl. Phys. **A603**, 257 (1996).
[14] L. Y. Glozman and D. O. Riska, Phys. Rep. **268**, 263 (1996).
[15] C. Hajduk and B. Schwesinger, Phys. Lett. **140B**, 172 (1984); B. Schwesinger, Nucl. Phys. **A537**, 253 (1992).
[16] F. E. Close, in *Spin and Isospin in Nuclear Interactions*, edited by S. W. Wissink, C. D. Goodman, and G. E. Walker (Plenum, New York, 1991), p. 75; T. Barnes and F. E. Close, Phys. Lett. **125B**, 89 (1983); Z. P. Li, V. Burkert, and Z. Li, Phys. Rev. D **46**, 70 (1992).
[17] P. Fuchs, W. Spang, and H. P. Morsch, *Proceedings of the International Conference on Physics with GeV-particle beams*, Jülich 1994 (World Scientific, Singapore, 1995), p. 258.
[18] P. Fernandez de Cordoba *et al.*, Nucl. Phys. **A586**, 586 (1995).
[19] S. Hirenzaki, P. Fernandez de Cordoba, and E. Oset, Phys. Rev. C **53**, 277 (1996).
[20] M. E. Sevior *et al.*, Phys. Rev. Lett. **66**, 2569 (1991); J. Lowe *et al.*, Phys. Rev. C **44**, 956 (1991).
[21] E. Byckling and K. Kajantie, *Particle Kinematics* (Wiley, New York, 1973).
[22] L. Lüke and P. Söding, *Springer Tracts in Modern Physics*, Vol. 59 (Springer, Berlin, 1971), p. 39.
[23] M. MacCormick *et al.*, Phys. Rev. C **53**, 41 (1996).
[24] A. Braghieri *et al.*, Phys. Lett. B **363**, 46 (1995).
[25] F. Härter *et al.*, Phys. Lett. B **401**, 229 (1997).
[26] R. A. Arndt *et al.* Phys. Rev. C **42**, 1853 (1990); **53**, 430 (1996).
[27] E. Oset and M. J. Vicente-Vacas, Nucl. Phys. **A446**, 584 (1985), and references therein.
[28] J. A. Gomez Tejedor and E. Oset, Nucl. Phys. **A571**, 667 (1994); **A600**, 413 (1996), and references therein.